Nanoscale

Accepted Manuscript

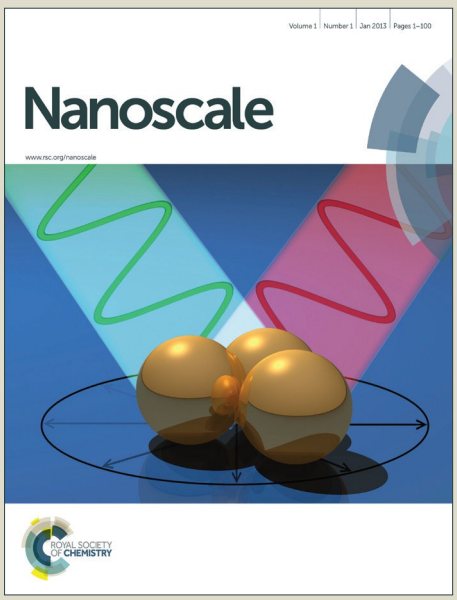

ROYAL SOCIETY OF CHEMISTRY

www.rsc.org/nanoscale

Oxidative addition of C−I bond on aluminum nanoclusters †

Turbasu Sengupta, Susanta Das* and Sourav Pal*

Energetics and in–depth reaction mechanism of the oxidative addition step of cross–coupling reaction is studied in the framework of density functional theory (DFT) on aluminum nanoclusters . Aluminum metal in its bulk state is totally inactive towards carbon–halogen bond dissociation but selected Al nanoclusters (size ranging from 3 to 20 atoms) have shown significantly lower activation barrier towards the oxidative addition reaction. Calculated energy barriers are lower than the gold clusters and within a comparable range with the conventional and most versatile Pd catalyst. Further investigations reveal that the activation energies and other reaction parameters are highly sensitive to the geometrical shapes and electronic structures of the clusters rather than their size, imposing the fact that comprehensive studies on aluminum clusters can be beneficial for nanoscience and nanotechnology. To understand the possible reaction mechanism in detail, the reaction pathway is investigated with the *ab initio* Born Oppenheimer Molecular Dynamics (BOMD) simulation and the Natural Bond Orbital (NBO) analysis. In short, our theoretical study highlights the thermodynamic and kinetic details of C-I bond dissociation on aluminum clusters for future endeavors in cluster chemistry.

1 Introduction

The C–C cross coupling reaction with transition metals as catalyst is the most promising tool of organic and material synthesis since the last four decades[1,2]. Bond formation process between two carbon atoms is highly energy demanding and hence a slow process[3,4]. Therefore C–C coupling reaction requires suitable catalyst to bring down the energy barrier and make the reaction practically viable with reasonably good chemical yield. Most extensively used catalysts are Cu, Ni and Pd complex[5–7]. Recent development in both experimental and theoretical contexts have shown Fe[8–10] and Au[11–13] perform moderately well in C–C cross coupling reaction. Among all these popular methodologies, most versatile and efficient catalyst for cross coupling reaction is the heterogeneous Pd(0) catalyst[14–16], commonly used via the different reaction schemes primarily developed by Kumada[17], Heck[18], Sonogashira[19], Negeshi[20], Stille[21] and Suzuki[14,22] in the early 70-80's. Heterogeneous Pd(0) catalyst not only gives good chemical yield with better product quality, but it is also reusable and most of the reaction schemes are less demanding[23]. Furthermore, most of the organo–palladium complexes are less sensitive towards moisture or air and also have high functional group tolerance. However, despite the above, Pd catalyst suffers from some well known disadvantages. Heterogeneous Pd catalyst is prone to catalyst poisoning and leaching[24,25]. Both Pd and Ni which are widely used catalyst for cross–coupling are highly expensive and poisonous, having low LD_{50} values[26,27]. Fi powder of Pd used as heterogeneous catalyst is pyrophoric as well[28].Therefore, finding an alternatives catalyst of Ni and P is the prime field of research to both theoreticians and experimentalists in recent years[16]. Among the newly developed alternative catalysts, both experimental[13,29] and theoretical investigations[30] have shown that Au nanoparticles can be used as an effective catalyst for C–C cross–coupling reaction. However, similar to Pd catalyst Au is also a rare element and highly expensive, which restricts its use for large scale industrial synthesis.

Al nanoclusters are well known for its reactivity[31–33]. Specifically, small sized aluminum clusters of 2–50 atoms are extremely reactive and show strong affinities to adsorb gaseous species such as H_2, D_2, O_2, N_2 and H_2O[34–38].The reactivity trends of open and closed shell aluminum clusters with oxygen are of great interest lately and experimental implementation[39–41] of the same is proven to be extremely influential in elucidating the role of spin conservation on the reactivity of aluminum clusters. Recent work by Castleman and Bergeron has shown that small sized aluminum cluster anions can dissociate the C–I bond of methy iodide with relative ease[42]. Scientists have also observed that MeI can be dissociated on Al(111) surface, confirmed by both scanning tunneling microscopy(STM) and DFT investigation[43]. Further analysis based on Jellium model reveals that specific Al clusters have some unique features. For example, Al_{13} cluster shows similarity with halogens, forms stable complexes with iodine[44], produces ionic assemblies with superalkali countercations[45,46], and even forms similar family of compounds comparable with polyhalides[47]. On the other hand, Al_7 shows both divalent and tetravalent valencies[48] similar to that of

† Electronic Supplementary Information (ESI) available: [Cartesian coordinates for the optimized structures and harmonic frequencies, Sample IRC data and plot, Grid data for Three Dimensional Potential energy surface and contour plot and Data for BOMD Simulation]

Physical Chemistry Division, CSIR–National Chemical Laboratory, Pune 411008, India

* *E-mail [Sourav Pal]: s.pal@ncl.res.in*

* *E-mail [Susanta Das]: susanta.chemistry@gmail.com*

carbon. All of these observations, stability and reactivity can neatly be explained by homogeneous electron gas (HEG) model or most commonly mentioned as *'Jellium model'* first used by Knight and co–workers[49] for similar context. These potent studies on Al clusters provoke further interest to judge their stabilities and reactivities for different chemical reactions and to observe and explain the effects of electronic structures, size and shape upon the energetics and mechanism. Detailed analysis can be useful and will have promising impacts in the field of nanoscience and technologies in the upcoming days.[50]Alongside these wide possibilities within the nano–regime, experiment and theoretical studies on atomic clusters can also be proven convenient in disclosing the long lasting queries about the bulk matter itself. Recently, Schnöckel and coworkers[41,51,52] have shown that oxidation reactions of Al_{13}^- cluster in HCl and Cl_2 environment can be treated as a precise micro analogue of the oxidation reaction of the bulk counterpart. Based on the state-of-the-art FT-ICR mass spectrometry they have evaluated each possible sub reaction steps of the oxidation process in both environment with absolute accuracy.Aside from the kinetic similarities regarding the products and intermediates, DFT investigation have shown astonishing thermodynamic resemblance in terms of exothermicity with the bulk metal for the same reactions. It is needless to say that in depth studies like these are of utter importance and definitely prospective in understanding the growth and form of bulk matter with atomic precision.

Fig 1 shows most common schematics[14] of cross–coupling reaction using Pd as catalyst. Other catalysts e.g Ni, Fe or Au follow similar mechanistic steps. The reaction proceeds via the oxidative addition of Pd(0) complex to organo–halide to form a Pd(II) complex. Next step is the transmetallation with another organometallic reagent where the nucleophile R′ is transferred from the metal to the Pd(II), which is the slowest step in the whole cycle and hence the rate determining step. The final process is the reductive elimination to give the coupled product (R–R′) and regeneration of the Pd(0) complex, to be ready for the next catalytic cycle. The overall catalytic reaction can be summarized as,

$$R - X + R' - M \xrightarrow{M'(0)} R - R' + M - X \qquad (1)$$

where M′=Pd,Ni,Au,Fe etc.

Oxidative addition is the process by which C–I bond dissociates and two separate bonds with the metal are created[3]. The opposite reaction is commonly known as reductive elimination. The process is reversible, but depending on overall thermodynamics, basicity of the metal and nature of the reactants, one particular direction is generally favored over the other one. Oxidative addition to a mononuclear complex increases the oxidation state of the metal center by 2, whereas for a binuclear metal catalyst, oxidation state of each metal center increases by one unit. One of the most amazing feature of oxidative addition is the wide range of reactants which can be involved in the dissociation process. Starting from highly polar molecule like organo halides or acids to totally non–polar molecule(H_2) can be dissociated with equivalent ease. The oxidative process can proceed via any of the four mechanistic pathways depicted in Fig 2. The first one is commonly know as the concerted mechanism, where breaking of C–I bond and formation of the bonds with the metals occurs simultaneously via a three member transition state. This process is common for non–polar molecules or aryl halides and followed by retention of configuration of corresponding stereogenic center. Unlike the concerted one, the S_N2 mechanism proceeds via the nuclophillic attack of the metal to less electronegative counterpart of the substrate leading to the cleavage of R–X bond in a organometallic cation, followed by coordination of X^- anion. This mechanism is mostly common for polar molecules and resulting retention of configuration of the stereogenic center. Third possibility of oxidative addition is through the ionic mechanism. This pathway is possible if the substrate (R–X) gets completely dissociated into two ionic fragments prior to the reaction. The overall mechanism can proceed via two following ways. First one is the attachment of R^+ fragment to the metal center, followed by subsequent coordination of X^- with the cationic complex. The alternative one is just the opposite where halide anion first coordinates with the metal center resulting an anionic complex with a rapid coordination of R^+ yielding the final product. The final one among the listed mechanism is non chain radical pathway[53]. The overall process in this mechanism is similar to S_N2 mechanism, only difference being that the fragmentation process generates radical species rather than ions, with the halide radical attaches itself with the organometallic radical. Rate of the reaction depends on the basicity of the metal, bond strength of R–X fragment and nature of substrate and solvent. The default rate of the reaction can further be influenced by modifying substrates, solvents or by adding foreign substances like radical scavengers[3], which in fact can even introduce radical pathway in a reaction which otherwise would have followed non–radical pathway. In some rare situations, two or more mechanistic pathway can participate in a competitive manner and the final outcome depends on the thermodynamics and the kinetics of each pathway and also on the imposed reaction conditions. Oxidative addition reactions of organo–halides are extensively studied and their mechanism is well established because of their importance in cross coupling reaction. The choice of halogens is usually in the order I > Br > Cl as C–X bond dissociation energy follows an opposite order[54] C–Cl($\sim$ 83 kcal mol^{-1}) > C–Br($\sim$72 kcal mol^{-1})> C–I($\sim$57 kcal mol^{-1}). Hence, iodine is the best leaving group among all the halides.

In this current article we have presented the thermodynamic

and kinetic details for the dissociation of C–I moiety on Al nanoclusters. Accurate DFT calculations shows that the Al nano clusters can participate in C–I bond dissociation, effective in both aliphatic and aromatic C–I bond cleavage. In addition with that in–depth reaction mechanism,detailed structural analysis and effect of shell structures of the clusters on the reaction controlling parameters are also properly accounted with BOMD simulation and NBO analysis.

The paper is organised as follows, in section 2 we have described in details the computational technique used. Section 3 deals with our results and elaborate discussion. Important conclusions are drawn in section 4.

2 Computational Details

All the clusters, Al_3, Al_5, Al_6, Al_7, Al_8, Al_{13} and Al_{20} in different possible conformations are optimized in the frame work of DFT using Gaussian 09 software package[55] with the TZVP basis set and B3PW91 functional. Only the lowest energy optimized structure in each case is chosen as one of the reactants in the C–I dissociation. All the organo–iodides (iodoethane, iodoethene and iodobenzene) are also optimized using same TZVP basis and B3PW91 functional for C and H similar to the prior case. However, for iodine, LANL2DZ basis is used in addition with LANL2 as model potential (pseudo potential) for the core electrons. Optimization of reactants and transition state are performed using Berny's eigenvalue following algorithm implemented in Gaussian 09 package. Normal modes of vibration of the optimized structures are carefully observed and it is made sure that all the energetically minimized structure (reactants) have no imaginary frequency whereas the transition states must and only have one single imaginary frequency of appropriate magnitude and which corresponds to the C–I bond itself. Intrinsic reaction coordinate (IRC) calculations are performed to confirm that the transition structures are connected with proper reactants and products along positive and negative direction of chemical reaction coordinate. Same calculations are further repeated using Minnesota functional M06–2X and also in double–hybrid BHandHLYP functional in an attempt to properly bracket the activation barrier for C–I dissociation on Al clusters. Thermodynamically controlled product of the reaction for each metal cluster was determined by calculating the energies of all possible products and choosing the energetically lowest conformer. Basis set superposition error (BSSE) are corrected using Boys and Bernardi's counterpoise correction scheme[56] within the Gaussian 09 software. Rate constants of C–I dissociation are calculated by using the Eyring–Polanyi equation[57–59]

$$k = \frac{k_B T}{h} e^{-\frac{\Delta G^{\ddagger}}{RT}} \quad where \quad \Delta G^{\ddagger} = G^{\ddagger}_{TS} - G_{Reactant} \qquad (2)$$

of transition state theory at 298 K and 1 atm pressure.
For a brief analysis of underlying reaction mechanism Natural Bond Orbital (NBO) analysis are performed on selected pre and post reaction complexes using NBO 3.0 suite implemented in Gaussian 09. NBO analysis are further used for each clusters separately to get the insight about stabilization of cluster during aromatic and aliphatic C–I bond cleavage on Al nanoclusters. The second order perturbative estimation of donor–acceptor stabilization energy(E_s) within the NBO basis are computed by

$$E_s = \Delta E_{ij} = q_i \frac{F_{ij}^2}{\Delta \varepsilon_{ji}} \qquad (3)$$

where q_i is donor orbital occupancy number. F_{ij} is off-diagonal elements of Fock matrix in NBO basis. $\Delta\varepsilon_{ji}=\varepsilon_j-\varepsilon_i$ is the orbital energy difference between acceptor(j) and donor(i) NBO.

Three dimensional potential energy surface scan is performed in B3PW91 functional and with the basis set described earlier in this section.The surface consists of a total 3111 grid points. 51 markers are assigned for C–I bond stretching along x axis and 61 are for increment of Al–I–C angle along y axis. Relaxed optimization are performed at each point without imposing any additional constraints. Energies(in a.u) obtained through the DFT calculation in each optimized points are plotted along the z axis. The surface is constructed by connecting all the plotted points in three dimensional Cartesian coordinate and a colormap is assigned based on the DFT calculated data range.

To gain further insight into the reaction mechanism we have carried out *ab initio* molecular dynamics simulation(BOMD) at room temperature (300K) using deMon.2.2.6[60] package. A total simulation time of 40 pico–second (ps) is introduced to assure that R–I molecule can have sufficient time to interact properly with the Al cluster. The temperature of the complex is maintained using the Berendsens thermostat (I = 0.5 ps) in an NVT ensemble[61]. The nuclear positions are updated using velocity Verlet algorithm with a time step of 1 fs. Throughout the whole simulation, we have fixed the total angular momentum of the cluster to zero, thereby suppressing the cluster rotation. Auxiliary density functional theory is employed for the BOMD simulations[62].

3 Results and Disscussion

To investigate the dissociation process of C-I bond on Al atomic clusters , we have chosen seven different atomic clusters of aluminum viz. Al_3, Al_5, Al_6, Al_7, Al_8, Al_{13} and Al_{20} keeping in mind that properties of atomic cluster are size and shape sensitive. Among them lowest energy conformers of Al_3 and Al_5 are planner and two–dimensional reflecting the

monovalent character of aluminum alike alkali metals in low coordination[63]. However, starting from Al_6 cluster becomes three dimensional as overlapping effect between s and p orbital becomes pronounced. As the second reactant we have selected three organo–iodides which are ethyl, ethylene and benzyl iodide respectively i.e. a combination of one alkyl, one alkene and one aryl halide of choice. Although calculations are performed in three different double hybrid DFT functionals B3PW91, BHandHLYP and M06–2X, during structural and binding energy comparison and also for Natural Bond Orbital (NBO) analysis we have followed the results obtained by M06–2X functional as family of Minnesota functionals are well known for good structural prediction as well as bonding interactions[64]. Structural parameters obtained in other two functionals are included in the **Supplementary Information (SI)**. Binding energies of the R–I molecule with Al clusters in all cases are calculated by the following formula $\Delta E = E(Al_n...IR) - E(R\text{-}I) - E(Al_n)$ All the thermodynamic parameters are calculated at 298 K and in 1 atm pressure.

The results and discussion section is divided into three parts. In the first part we have discussed structural and thermo–chemical aspects of C–I dissociation on selected Al clusters based on DFT investigation. Second part of the discussion includes the mechanistic aspects of oxidative addition over Al cluster based on the DFT calculation and the natural bond orbital(NBO) analysis. The findings of Born Oppenheimer Molecular Dynamics simulation of C–I bond activation upon Al cluster are further included in this section. One of the important features of atomic clusters is that each cluster can behave drastically different from each other. The major reason lies behind is the electronic and geometric shell effect of the cluster itself, commonly known as the cluster size effects(CSE)[65]. CSE of a cluster can uniquely change the reactivity of each member of same cluster family, and as a result all the parameters including thermochemistry, reaction mechanism and structure of reactants and products can be abruptly different for each member, even for the same reaction. Due to above fact, we have tried to emphasize on each cluster while discussing in details. Specific observations which may be caused by CSE are also duly noted and attempted to explain accordingly. Third part provide the comparison of our result with experimental and theoretical results available in modern literatures. Fourth section comprises remarks and final conclusions.

3.1 Structural and Thermochemical aspects

We begin our discussion with the two smallest clusters of our study which are Al_3 and Al_5. As mentioned earlier, both these clusters are two dimensional having very high surface to volume ratio. Hence, it is expected that both of these cluster should be more reactive and hence will show low activation barrier. Table 1–6 compiles all the thermodynamic data including rate constants and binding energy for all three organo–iodides. It is evident from the table that for all three cases both Al_3 and Al_5 indeed have shown low activation barrier and very high rate constants in all three functionals. Results obtained in B3PW91 functional is usually less than other two functionals, in some cases estimated barrier in B3PW91 functional is lower by factor of two or three when compared with the results obtained in other two functionals. An activation energy($\Delta G^{\ddagger}$) of 1.8 kcal mol^{-1} in B3PW91 functional is also observed for ethyl iodide on Al_3 cluster, which is the lowest activation barrier reported within the study (therefore highest rate constant of magnitude $\sim 10^7$ unit) ,whereas same parameter predicted by other two functionals is much higher. This trend is also observed in other clusters which seems to raise a suspicion that results obtained in B3PW91 functional seem to underestimate the activation barrier. Underestimation of activation barrier is not uncommon for B3PW91 functional and DFT investigations have shown that other double hybrid functional like BHandHLYP performs better in such cases[66]. Although it must also be mentioned, that this underestimation seems to be less pronounced for bigger clusters and in some rare cases activation barrier obtained in B3PW91 function is closer with M06–2X result (e.g. dissociation of iodoethene on Al_8 cluster) than BHandHLYP functional.

Comparison of the reactivity of Al_3 cluster with Al_5 cluster is not as straight forward as comparing its reactivity with other members within our study. According to the jellium model considering the monovalent character of aluminum in this size scale, Al_3 cluster has a total of 3 valence electrons ,one electron higher than the magic number 2 due to 'S' Jellium shell closing. Hence a low activation barrier for oxidative addition is expected as the cluster achieves the stable filled shell magic cluster configuration upon one electron loosing. So, based on the argument Al_3 cluster should be more reducing than Al_5 cluster as this stability driven electronic shell effect is absent in later case. This prediction is proven correct for ethyl iodide(Table 1 and Fig 6 (a)). Both $\Delta G^{\ddagger}$ and $\Delta H^{\ddagger}$ values for Al_3 cluster are lower than Al_5 cluster for all three functionals. However, the same cannot be said for other two iodides. Results obtained for iodoethene and iodobenzene in all three functionals are too close to comment about their exact reactivity order towards oxidative addition of C–I bond. As a matter of fact, inclusion of other factors like nature of the reactants(iodides), geometrical stability of clusters and structure of transition states are necessary to conclude their relative reactivity. It is evident that all of these factors cumulatively determine the magnitude of the activation barrier rather than the electronic shell effect alone.

All the other clusters within our study are three dimensional with relatively higher surface to volume ratio than Al_3 or Al_5 Most of them have shown comparatively higher activation bar-

rier than the planner ones as expected(Table 1–6). Only exception is the Al_7 cluster which have shown exceptionally low activation barrier for all three iodides in all three functional. Computed activation energies of Al_7 cluster is comparable with planer clusters or even lower than that of Al_3 and Al_5 clusters. Explanation of this unusual behavior can again be given from jellium picture. According to the jellium model, electronic structures of Al_7 and Al_3 cluster are similar. Al_7 cluster has 21 valence electrons, one electron more than closed shell configuration(20). Hence, similar to that of Al_3 cluster, it is expected that Al_7 cluster should show low activation barrier towards oxidative addition. This conclusion further proves the fact that unlike the case of Al_3, electronic shell effect is the dominant factor for the reactivity of Al_7 cluster. Among all the clusters Al_7 has shown the second lowest activation barrier($\Delta G^{\ddagger}$ of 2.8 kcal mol^{-1}) and second highest E.P rate constant of order $\sim 10^{10}$ unit for iodoethene in B3PW91 functional. In spite of these exceptional behavior of Al_3 and Al_7 due to electronic shell effect(ESE), the activation barrier seems to increase with increase in the size of the cluster, as expected, which after a particular size scale would eventually render the cluster completely ineffective towards the oxidative addition, as observed in bulk phase. Thus, based on all three functionals Al_{20} cluster on average shows highest activation barrier and hence lowest rate constants among all the clusters listed. Fig 6(a) collects activation free energies for ethyl iodide in all three DFT functionals. It is prominent from the oscillatory nature from the plot that 'Shell effect' is indeed the key factor which determines the chemical reactivity of aluminum clusters towards oxidative addition. As mentioned earlier all the clusters having number of valence electron higher by one unit than the closed jellium shell configuration shows lower activation barrier and higher rate constant than the rest of the members. This observation is indeed consistent with the experimental findings obtained by Castleman and Bergeron[42], where the reactivity of the cluster anion is found to be inversely proportional with the electron affinity of them and Al_{13}^- is found to be least reactive.The chemical inertness of Al_{13}^- is also observed in the acid dissolution experiment performed by Bowen, Schnöckel and coauthors[41,51]. Even with strong acid like hydrochloric, Al_{13} cluster anion is found to be resistant towards oxidation due to the presence of highly endothermic intermediate reaction steps.Hence, in order to initiate the cascade of acid leaching reactions, additional energy input via radio–frequency (RF) pulse is observed to be essential. Similar behavior is again reflected in experiment with Cl_2[41,52],O_2[39–41]as well as NH_3[67] environment. The chemical inertness of Al_{13}^- can again be attributed to its filled shell magic number(40) configuration alike to the present study.

Moving to the exothermicity values, first thing to observe from Table 1–6 is both the Δ G and Δ H values for all clusters are highly negative. When compared by magnitude, the exothermicity values are nearly double or triple than the ΔG and ΔH values obtained for gold clusters in the same functionals[30]. Highly negative ΔG values indeed indicate enhanced spontaneity of the reaction in accordance to thermodynamic principles and high exothermicity(ΔH) proves higher thermodynamic stability of the post reaction complexes. One important observation in all the cases of our study is that the change in Gibbs free energy of the reaction (ΔG) values are always greater than change in enthalpy of reaction(ΔH) values. Hence, the reaction is entropically unfavorable, which is expected in case of oxidative addition. Brief investigation using NBO analysis reveals that principle reason of this high exothermicity is intra–cluster stabilization in the post reaction complexes. NBO calculation indicates that all the post–reaction complexes are highly stabilized by multiple newly introduced donor acceptor(Al–Al) interactions which were either absent or have negligible contribution in the pre–reaction complexes. For example, for the reaction of iodoethane on Al_3 cluster we have found two newly introduced Al(LP)–Al(LP*) donor acceptor interactions of magnitude 72.6 and 122.1 kcal mol^{-1} respectively in the post–reaction complex, whereas no Al(LP)–Al(LP*) interaction with stabilization energy contribution higher than 32 kcal mol^{-1} is found in the pre–reaction complex for the same. Similar intracluster interactions are also observed for other clusters within the list as well. This signifies that the cluster gets more stabilized via intra–cluster donor acceptor interaction upon attachment of the fragmented R–I moieties after the dissociation process. This is the prime reason of high exothermicity and high spontaneity of the dissociation process. Fig 9 shows pictorial representation of some of these intracluster interactions with their respective stabilization energies for different clusters. Plotting the exothermicity values with cluster size(Fig 6 (b)) shows similar oscillatory pattern as obtained in case of activation energies in all functional and for all three organo iodides. The exothermicity pattern again reflects the importance of electronic shell effect on determining their chemical behavior.

In this context it is interesting to look upon the geometrical or structural stability of the aluminum clusters. All the structures of pre and post– reaction complexes are included figure 3, 4 and 5. It is evident that upon attachment of R and I group, all of the small sized (Al_3–Al_8) clusters get structurally distorted. Only exception is the Al_3 cluster which due to having a planer three membered ring, is unable to release the strain (Baeyer's strain) via out–of–plane bending. Hence, only distortions which are observed for Al_3 cluster are mostly consists of bond length or angle distortions. Except Al_3 cluster, all the other clusters upto Al_8 show significant distortions in the post–reaction complexes upon R–I attachment. Most notable among them is the dramatic structural change of Al_5 cluster which, in its lowest energy conformer, is planer but changes to a distorted pyramidal shape in the post reaction complex as ev-

ident from Fig 3. On the contrary bigger clusters Al_{13} and Al_{20} are mostly found resistant to structural changes (Fig 5). Al_{13} is a 13 atom icosahedral cluster, icosahedral shape is well known for its high stability and the key factor to control the geometrical stability in cluster chemistry. On the other hand structure of Al_{20} cluster can easily be constructed by combining two Al_{13} clusters on top of each other and removing the pentagonal pyramidal cap of the lower cluster. These unique shapes of both Al_{13} and Al_{20} are the key reasons of their structural integrity. Except some minor distortions,the icosahedral cores of both the Al_{13} and Al_{20} clusters are found to be totally intact in the post–reaction complexes.That proves that unlike the case of HCl and Cl_2 [41,51,52]icosahedric Al clusters are structurally resistant towards leaching by the organo–iodides, which is, as a matter of fact is also proven by related experiment[42].

Tables 2, 4 and 6 collect binding energy values calculated in M06–2X functional for all three iodides calculated using the formula mentioned earlier. Binding energy values represents the strength of Al–I bond in the pre–reaction complexes. Binding energy values are significantly lower than that of gold clusters, which can be explained improvising the fact that position of aluminum in the periodic table is in period 3, whereas gold (Au) an element of period 6 lies much closer with iodine (period 5). Hence, binding of iodine will be more stronger with iodine than aluminum due to better orbital matching. In our case, binding energy values on aluminum clusters for all thee iodides lies within the range $\sim$ 1 kcal mol^{-1} to $\sim$ 10 kcal mol^{-1}. Highest BSSE corrected binding energy value is obtained in case of Al_6 for iodoethane which is 8.9 kcal mol^{-1}. Based on our DFT calculations on all three reactants and in M06–2X functional, Al_6 cluster shows better binding energy(ΔE_{BSSE} 7.6–8.9 kcal mol^{-1}) than rest of the clusters. Trends in binding energies also follow the same random pattern like activation energy and exothermicity values signifying that CSE is the dominant factor in this case as well.

3.2 Reaction mechanism

To understand the details of the reaction mechanism of C–I bond dissociation on aluminum cluster, we have performed natural bond orbital (NBO) analysis and Born Oppenheimer Molecular Dynamics(BOMD) simulation along with the DFT calculation. Second order perturbation treatment of Fock matrix in the NBO basis usually provides information about most stabilizing donor–acceptor interaction between Lewis acid–base pairs which are present within the chemical species. On the other hand, BOMD calculation can simulate and interpret the dissociation process of C–I bond on aluminum cluster in real time. Observation based on frontier molecular orbital shows that in each case organo–iodides bind with aluminum cluster utilizing its lone pair electron density. Fig 7 shows the frontier molecular orbitals for the pre reaction complexes of both Al_3 and Al_5 cluster. Minor contribution from π electron density of iodoethene and iodobenzene can be observed from the figure. NBO analysis indicates a stabilization energy contribution of about 13.48 kcal mol^{-1} due to donor–acceptor interaction between nonbonding orbital(LP) of iodine in iodoethane to antibonding orbital (LP*) of Al_3 cluster. In case of iodoethene and iodobenzene on Al_3 stabilization energy values due to I(LP)–Al(LP*) interaction are found to be 10.86 kcal mol^{-1} and 7.31 kcal mol^{-1} respectively. The I(LP)–Al(LP*) stabilization energy for Al_5 cluster with ethyl iodide is 16.8 kcal mol^{-1}, for ethylene iodide it is 8.2 kcal mol^{-1} and in case of benzyl iodide which is 9.5 kcal mol^{-1} intermediate of the previous two values. Despite the fact that the frontier orbital picture indeed shows participation of π electron density in the bonding process with the cluster, NBO analysis shows no significant stabilization due to this interaction. In fact, no donor acceptor stabilization energy value more than 2 kcal mol^{-1} is obtained due to π electron participation to aluminum cluster. This result confirms that the dominant contribution to the stabilization of the pre–reaction complexes is due to the interaction between lone pair of iodine and with the cluster itself. The π electron density induces negligible effect in the binding energies.

The stabilizing interactions of iodine with the cluster are slightly different in post–reaction complexes of C–I dissociation. As observed from Fig 8, that in the pre–reaction complex of Al_3 and iodoethane the donor acceptor interaction are of σ type i.e. the orientation of non–bonding orbital of iodine and antibonding orbital of aluminum are along a common axis. However, this interaction changes to a parallel or π interaction in the post–reaction complexes can be seen from Fig 8. Although it seems that interchanging the orbital orientation barely affects the stabilization energy contributions. In all three post–reaction complexes of Al_3 cluster the I(LP)–Al(LP*) stabilization energies are in the range 11.3–11.4 kcal mol^{-1}, whereas for Al_5 cluster these values are within 8.5–12.0 kcal mol^{-1} for all three iodides. Binding of Carbon fragment in the post–reaction complex differs with that of iodine by two ways. Firstly,donor–acceptor stabilization energies are manyfold higher than that of iodine with aluminum. As for example C(LP)–Al(LP*) stabilization energies for ethyl, ethylene and benzyl iodide with Al_3 cluster are 71.6,83.1 and 66.1 kcal mol^{-1} respectively. The principle reason lies in the fact that both carbon and aluminum lies much closer in the periodic table, hence orbitals are well matched energetically as well as coefficient wise. Therefore the overlap between the NBO orbitals of carbon and aluminum is more effective resulting in higher stabilization energy contributions. Second major difference is that unlike the case of iodine which can only be stabilized by only one type of donor acceptor interaction(I(LP)–Al(LP*)), NBO calculation shows carbon can produce multiple types of donor acceptor interactions varied in stabilization

energy, for example Al_7 cluster The Al...C bond is stabilized by an amount of 21.5 kcal mol^{-1} due the interaction between non–bonding orbital of Al(n) and sigma antibonding interaction (Σ^*) of Al–C bond. This interaction is unique and not observed in any previous cases.

To further investigate the reaction in details, part of the potential energy surface is constructed for the reaction between Al_3 cluster and iodoethane in B3PW91 functional and in the given basis. Due to computational constraint and high exothermicity of the reaction (the post–reaction complex lies far below in the potential energy surface) only most significant portions of the surface is evaluated. Position of both pre–reaction and the transition states are evident from Fig 10. The right hand contour plot clearly shows that point C, which is the path towards the post–reaction complex is connected with the pre–reaction complex (point A) by a first order saddle point B.The geometry of the system at point A and B, evaluated from the potential surface calculation are indeed matches exactly with the optimized structures of pre–reaction complex and the transition state obtained by B3PW91 calculation as mentioned before(see **Supplementary Information**). As shown in the right hand contour plot that point A, B and C can be connected via a possible minimum energy path (MEP) directing towards the post–reaction complex of the reaction. Fig 11 and 12 concludes the result obtained by Born–Oppenheimer Molecular Dynamics (BOMD) simulation of iodoethene on Al_5 cluster. The BOMD simulation demonstrates that after absorbing on Al surface R–I molecule undergoes several orientations until dissociates as shown in figure 11. The starting geometry for MD simulation at 0 picosecond(ps) is the M06–2X optimized geometry of the reactant of iodoethene on Al_5 cluster. In the initial sturture at 0 ps the Al–I and I–C bond lengths are found to be 3.61*Å* and 2.10*Å* respectively. The C–I bond oscillate between 2.2 *Å* to 3.1 *Å* during the initial simulation steps upto 34 ps then it rapidly increases and finally dissociates at 34.6 ps as clearly observed from the plot of C-I bond length (in *Å*) versus time(ps) in Fig 12 .

3.3 Comparison with reported values

Comparison of the results obtained within the present study with other results available in literature is essential in order properly understand the reactivity of small sized aluminum cluster towards C–I bond dissociation. Based on recent literatures, it is nearly impossible to quantitatively compare the results due to two prime reasons. Firstly, theoretical results obtained are often calculated in different theoretical levels with variable accuracy. As a second reason, it must be said that, there is certainly some limitation in terms of experimental context. As atomic clusters are extremely small particles ranging even within sub–nano level and also metastable in nature, there is difficulty associated to properly predict the structure and nature of reactants and products by experimental means. Hence, data obtained by experimental methods are rare and suffer from uncertainties due to the unstable nature of nano–clusters and there discrete size.

In spite of all these, it is still possible to compare and conclude qualitatively based on the data available in the literature. As mentioned in the introduction section, Corma and coworkers[13,29] have studied extensively the sonogashira cross–coupling on gold nanoparticles supported on cerium oxide(CeO_2) nanocrystals. Their study also includes the DFT calculated activation barrier for iodobenzene on Au_{38} cluster in PW91 functional which is 11.3 kcal mol^{-1}. Further study using B3PW91/6–31G(d,p) level of theory indicated that this activation barrier is much higher (31.6 kcal mol^{-1}) in Au^I complexes(Me_3PAuI) when compared to Au_{38} cluster. A more detailed DFT investigation is performed by Dutta *et al.*[30] for the dissociation of ethyl, ethylene and benzyl iodide on neutral and positive charged clusters ranging from Au_3 to Au_{20}, much similar to our calculation. Their overall investigation is comprises of two types of DFT calculations in B3PW91/TZVP, LANL08(Au,I) and M05–2X/6-31+G(d), LANL2DZ(Au,I) level of theory. The maximum activation barriers obtained for neutral Au cluster in their calculation are 26.2 and 32.6 kcal mol^{-1} with an average of 18.2 and 24.5 kcal mol^{-1} at two levels of theory respectively. In both levels the lowest free energy barrier(8.7 and 11.5 kcal mol^{-1} respectively) is calculated for iodobenzene on Au_3 cluster improving the fact that small Au clusters are more reactive than the larger ones. Inclusion of results obtained for charged cluster within this data only barely affects the average activation barrier and maximum and minimum free energy barriers are not altered at all. Fig 13 shows a qualitative comparison column plot between the free energy barrier($\Delta G^{\ddagger}$) obtained for Au clusters with the results obtained for Al clusters in this current study. Qualitative comparison between two different set of DFT functionals proves the superiority of the results obtained for aluminum cluster than gold cluster. In both set of data aluminum cluster shows lower activation energy in all three categories which are maximum, minimum and average energy of activation. In B3PW91 functional aluminum clusters show an average free energy of activation of 11.1 kcal mol^{-1} with 22.6 kcal mol^{-1} and 1.8 kcal mol^{-1} being the maximum and minimum activation energy respectively. Similarly The maximum, average and minimum $\Delta G^{\ddagger}$ for Al clusters in M06–2X functional are found to be 29.9, 3.4 and 14.7 kcal mol^{-1}, much better than the results obtained for gold cluster mentioned earlier.

Comparison of our results with Pd cluster is more difficult because of the wider range of Pd contained complexes used in cross coupling reaction. Pd complexes usually shows a range of activation barrier starting from very low to medium activation free energy depending on type of ligands attached with

them and the reactants which are used. The different dissociative pathway can also differ in activation barrier in significant manner. Based on these facts activation barrier calculated for Pd catalyst also consists of broad range rather than a slender one. Available literature shows that concerted dissociation of C–I bond on Pd catalyst via a three member transition state shows an activation energy of 17 kcal mol^{-1} [3]. On the other hand, Bickelhaupt and de Jong, based on their gas phase relativistic DFT calculation, have shown that the activation barrier calculated by activation strain model for C–I bond dissociation via a S_N2 pathway with rearrangement on Pd catalyst is as low as 10 kcal mol^{-1} [68]. Calculated average activation barrier by two different functionals for Al cluster(11.1 and 14.7 kcal mol^{-1}) lies closer within this range as mentioned above.

4 Conclusion

Present study includes a theoretical investigation of oxidative addition of C–I bond over Al clusters combining both Density functional theory and molecular dynamics methods. C–I bond dissociation is indeed a crucial reaction and provides a key step in various important organic reactions like cross–coupling. Most commonly used catalyst are d and f block elements like Pd, Ni, Cu, Fe and Au. Our investigation shows that although Al, which is a p block element is ineffective to dissociate the carbon–halogen bond in bulk phase, nano–clusters are found to be highly effective for the same. Calculated activation barriers reveal that Al nano–clusters are remarkably efficient towards C–I bond activation and dissociation. In terms of activation barriers and exothermicity, aluminum clusters have shown better results as compared to Au clusters. The calculated activation barriers are also within the range shown by the most versatile and efficient Pd catalyst. Further observation reveals that the reactivity of aluminum clusters in terms of activation barriers and other reaction parameters are highly dependent on the electronic (Jellium) shell configuration of the clusters, an observation consistent with the experimental findings.[39–42,51,52,67] This indeed concludes that effective reactivity can also be obtained in selected bigger clusters or even in solid supported clusters. Our study highlights a brief analysis including structures and stabilities of the reacting species along with the thermochemistry and mechanistic pathway of the reaction which may be proved highly useful for future experimental implementation for similar purposes. Al clusters have long been known for their high reactivity, as proven numerous times by both experiments and theory, our investigation also suggests that in cluster state aluminum can be equivalently reactive even as the transition metals. With the technological and experimental progress in nano–cluster synthesis, separation and stabilization, such fundamental studies based on the reactivity and stabilities of aluminum clusters may be proven rewarding and will no doubt be highly beneficial in disclosing the deepest secrets within the nano-regime.

5 Acknowledgement

T.S. acknowledges UGC (University Grant Commission) for JRF (Junior Research Fellowship). S.D. acknowledges CSIR (Council of Scientific and Industrial Research) for funding of the SRF (Senior Research Fellowship). We acknowledge the Center of Excellence in Scientific Computing at CSIR – NCL and the CSIR 12^{th} five year plan MSM project (csc 0129) grant. S.P. acknowledges grant from the SSB project of CSIR and the J.C. Bose Fellowship grant of DST towards partial fulfillment of this work.

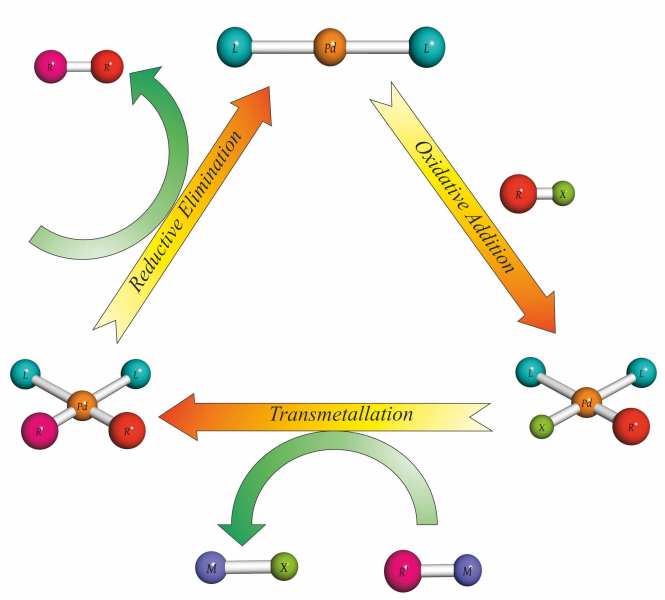

Fig. 1 A common scheme for cross coupling reaction cycle using Pd as catalyst. The transmetallation step is the slowest step and hence the rate determining step.

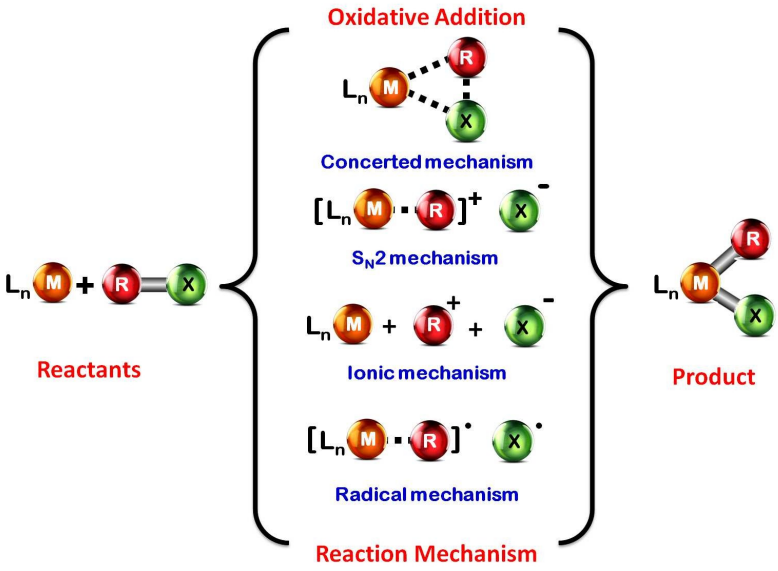

Fig. 2 All the possible reaction mechanisms for the oxidative addition of organohalides with metal catalyst.

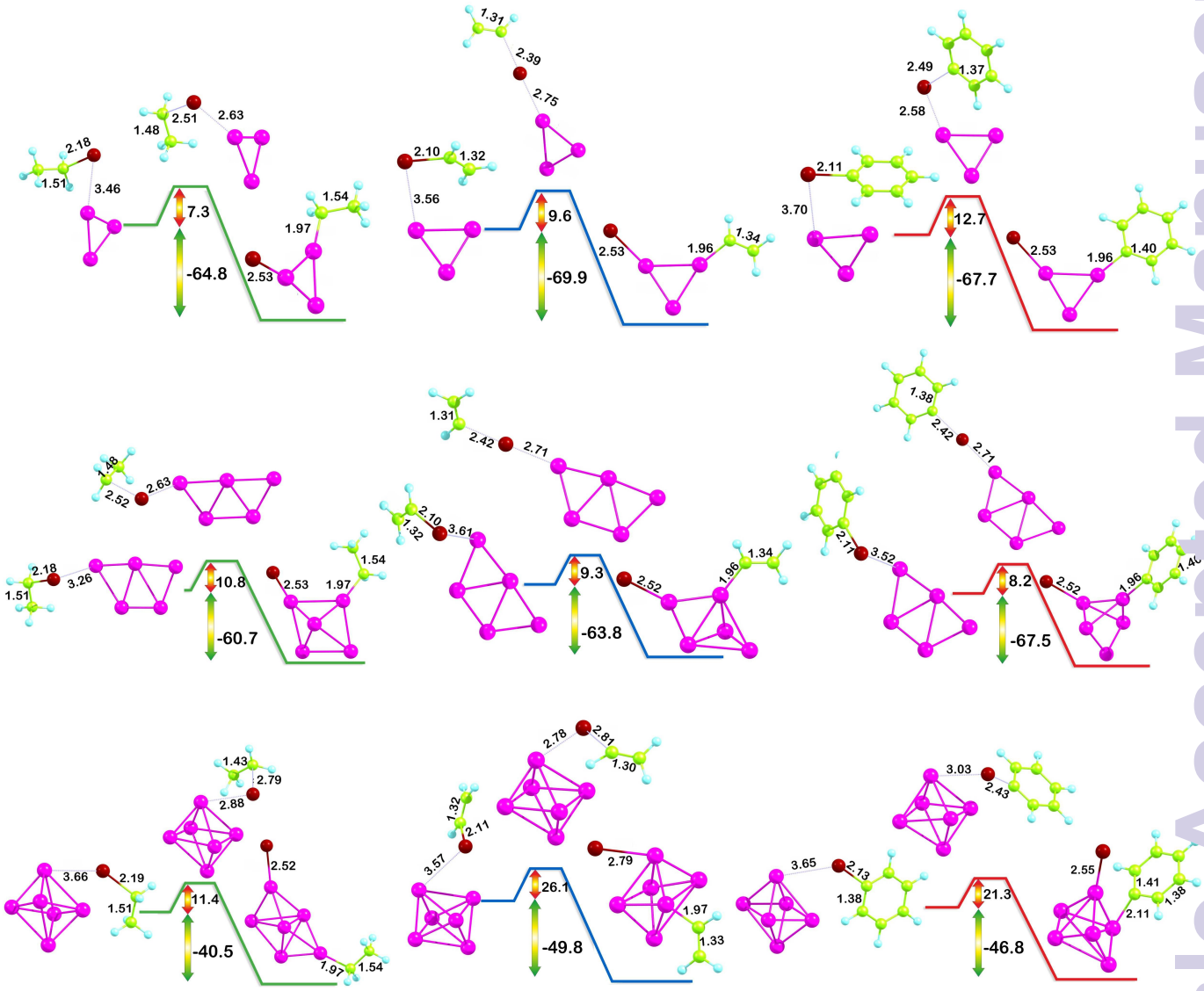

Fig. 3 Energy profile diagrams for Al_3-Al_6 clusters for all three iodides.Orange arrow highlights the activation barrier ($\Delta G^{\ddagger}$) and green arrow highlights corresponding exothermicity(ΔH) in M06–2X functional

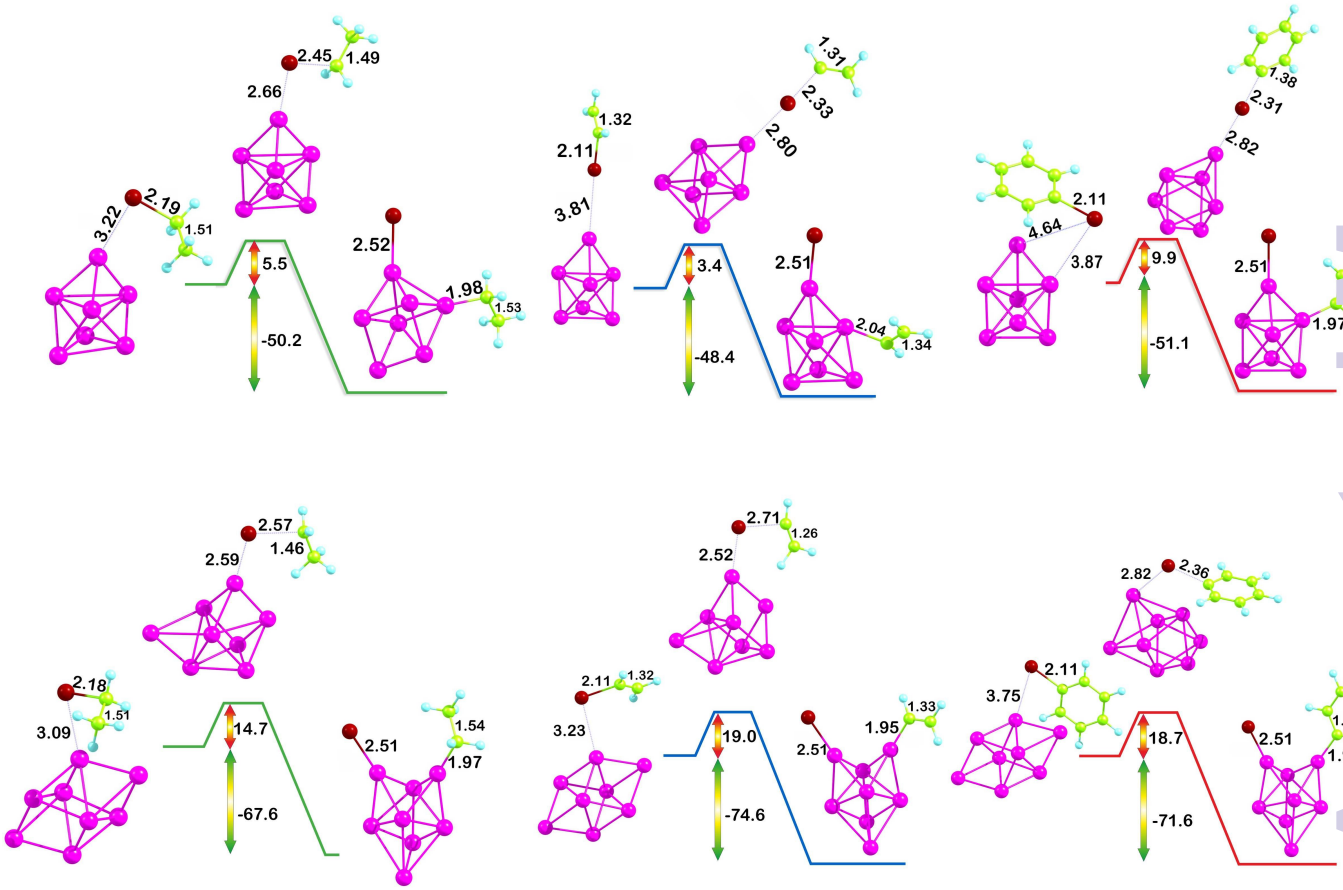

Fig. 4 Energy profile diagrams for Al_7 and Al_8 clusters for all three iodides.Orange arrow highlights the activation barrier ($\Delta G^{\ddagger}$) and green arrow highlights corresponding exothermicity(ΔH) in M06–2X functional

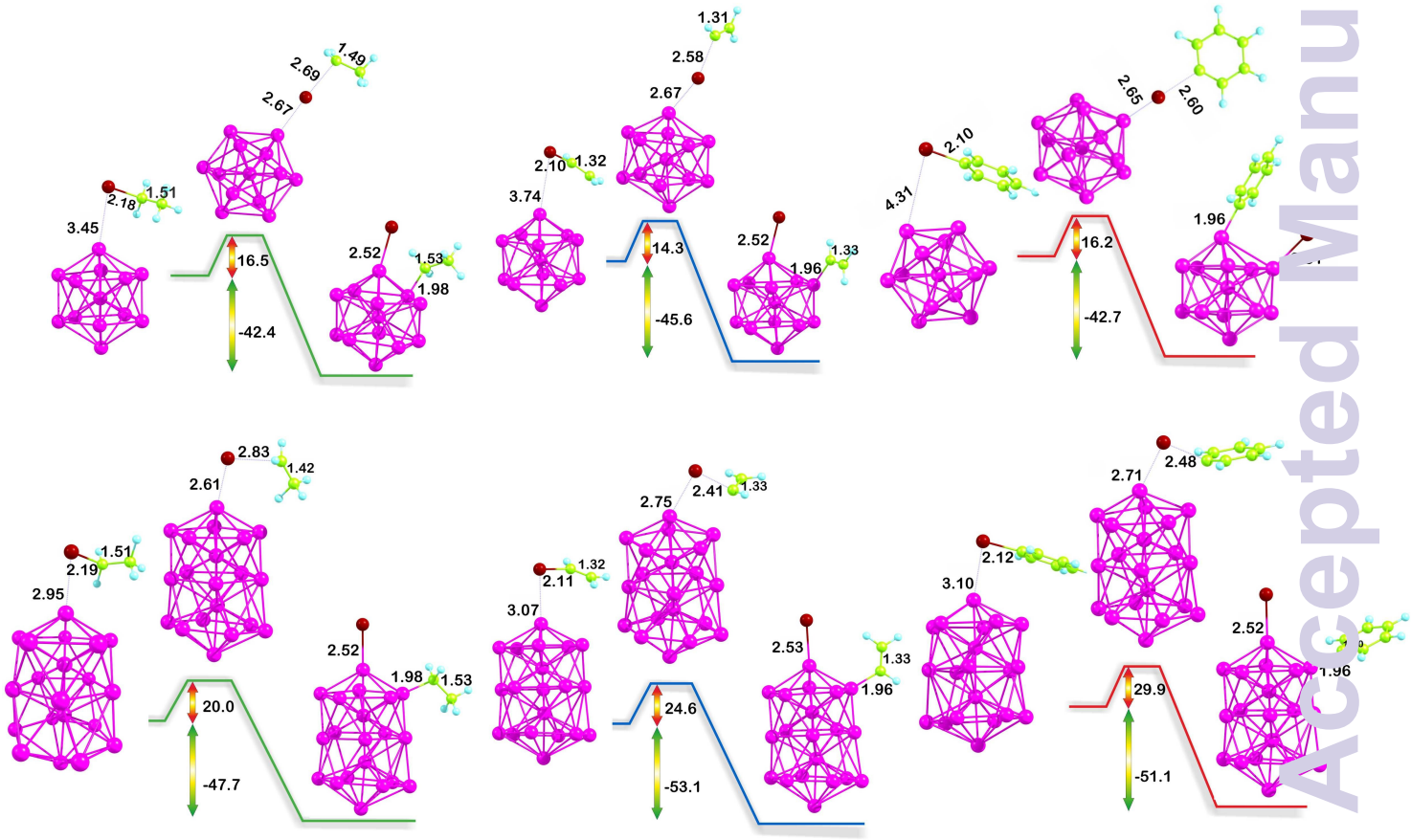

Fig. 5 Energy profile diagrams for Al_{13} and Al_{20} clusters for all three iodides.Orange arrow highlights the activation barrier ($\Delta G^{\ddagger}$) and green arrow highlights corresponding exothermicity(ΔH) in M06–2X functional.

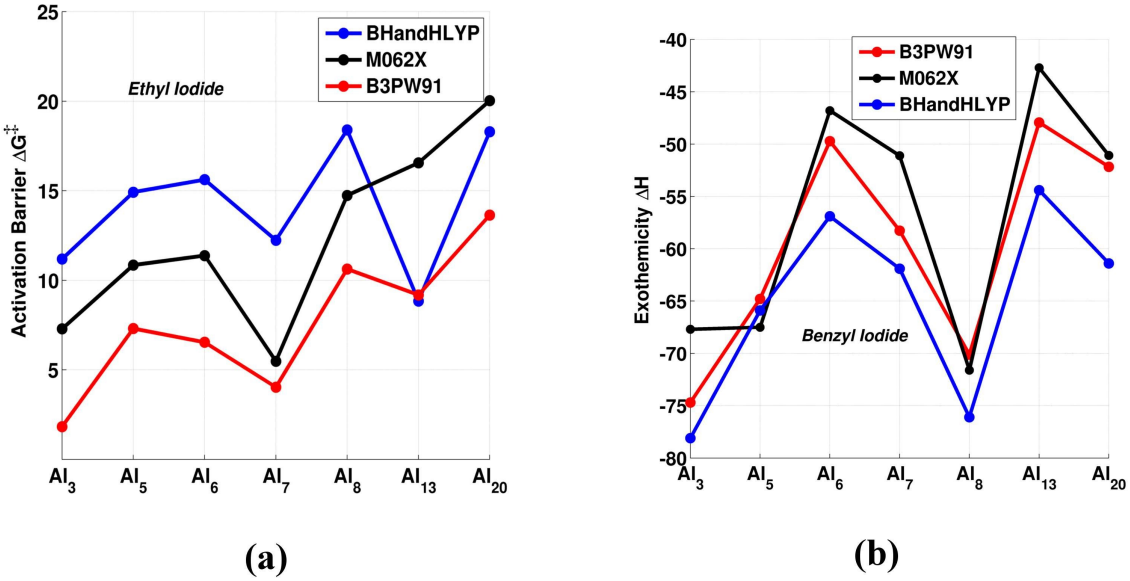

Fig. 6 Plot of activation energies (a) for ethyl iodide and exothermicities (b) for benzyl iodide in all three functionals.The random trend shows strong influence of *'Shell effect'* on both the parameters. Low activation barriers (a) for Al_3 and Al_7 can be explained by invoking the concept of spherical *Jellium shells*.

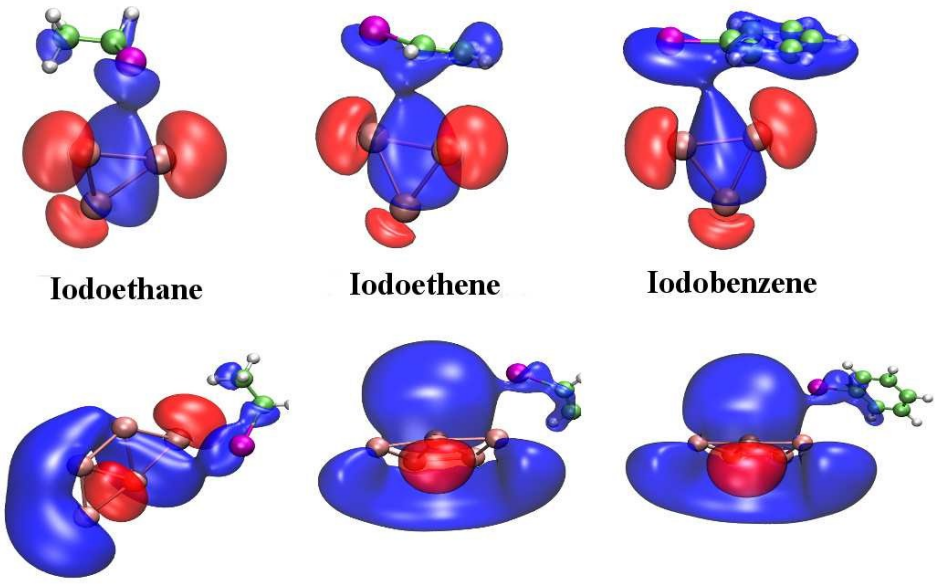

Fig. 7 Frontier molecular orbitals of pre–reaction complexes of Al_3 and Al_5 cluster with all three iodides. In all cases iodine binds with Al cluster utilizing its lone pair. In specific cases minor contribution from π electrons (for ethylene and benzyl group) are also observed.

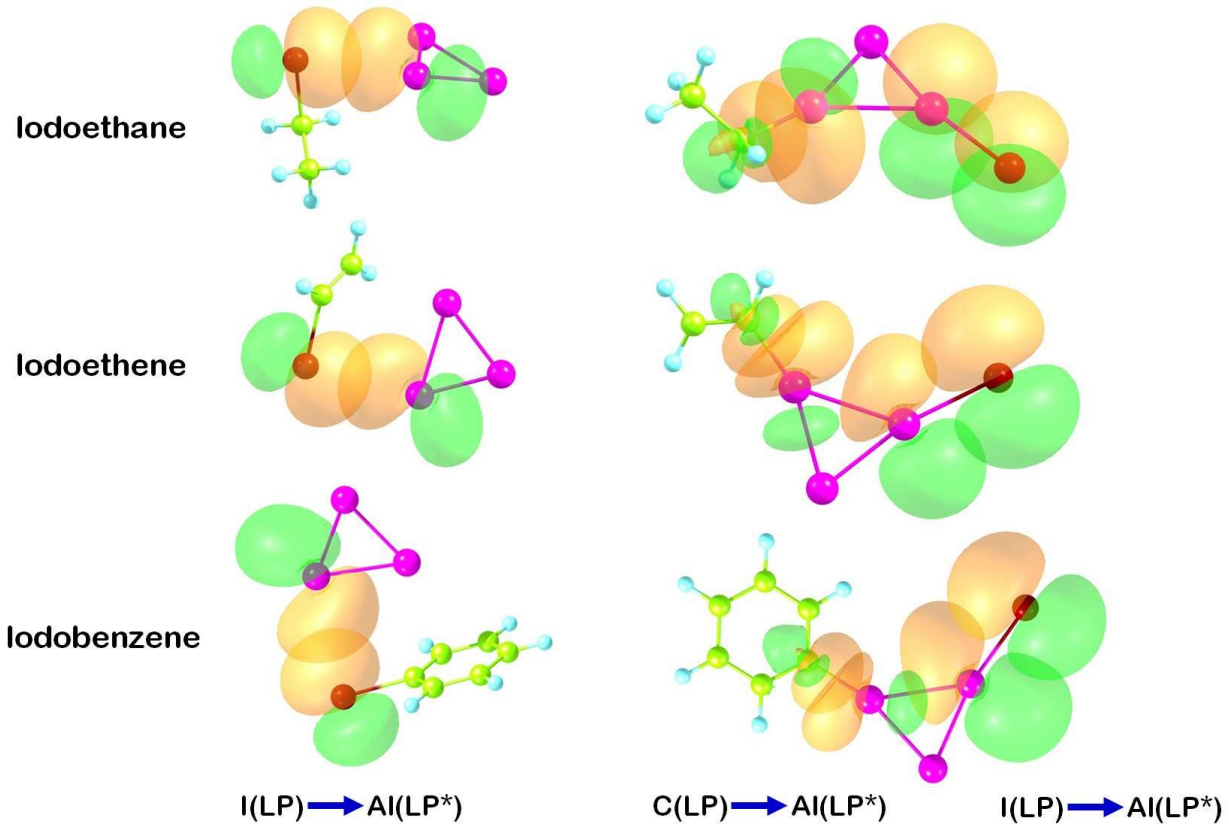

Fig. 8 Most stabilizing donor–acceptor interactions for pre and post reaction complexes of Al_3 cluster as indicated by NBO analysis.

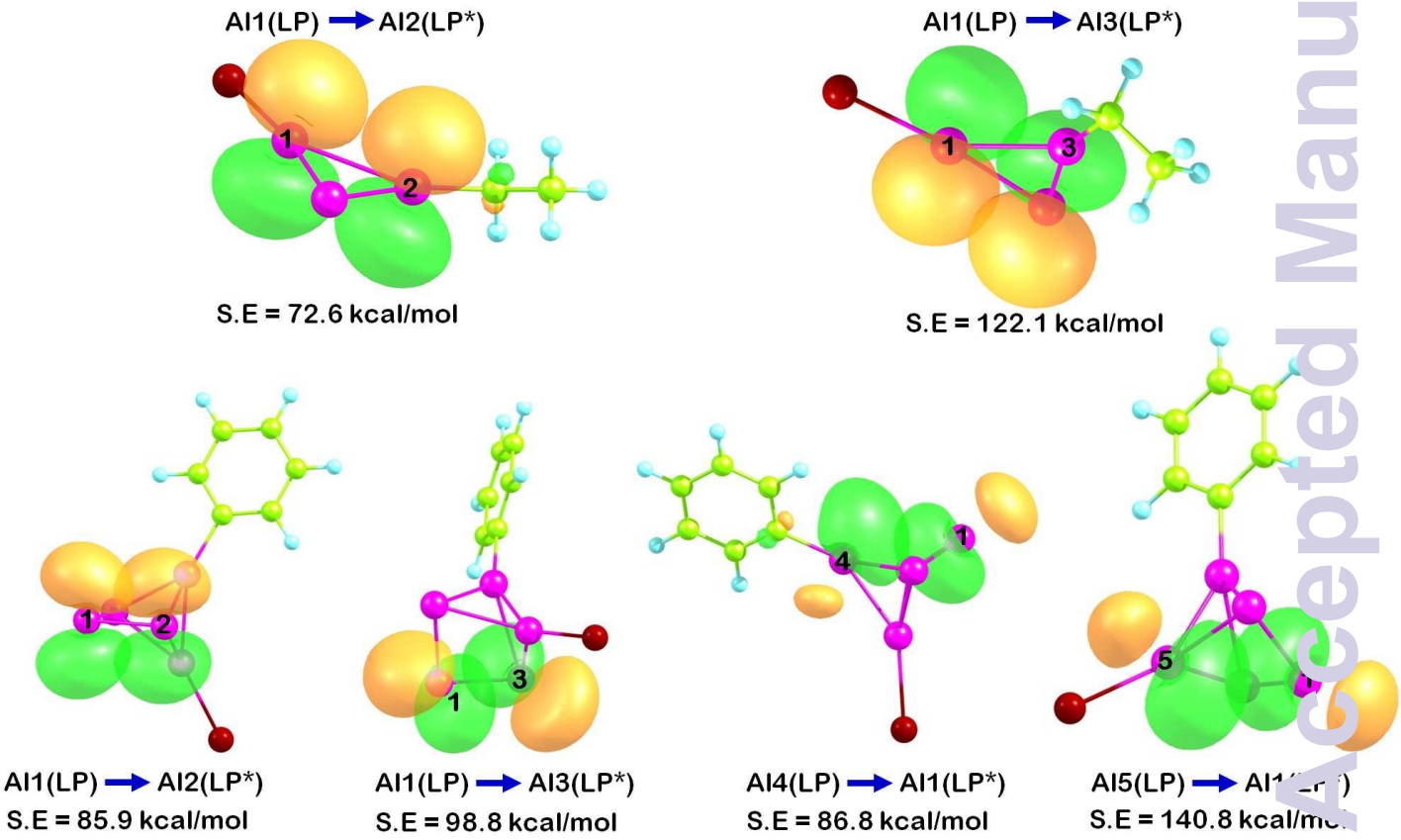

Fig. 9 Most stabilizing intracluster donor–acceptor interactions in the post–reaction complexes for Al_3(iodoethane) and Al_5(iodobenzene) are shown as indicated by NBO analysis. These intracluster stabilization are the reason for the high exothermicity as indicated by DFT calculation.

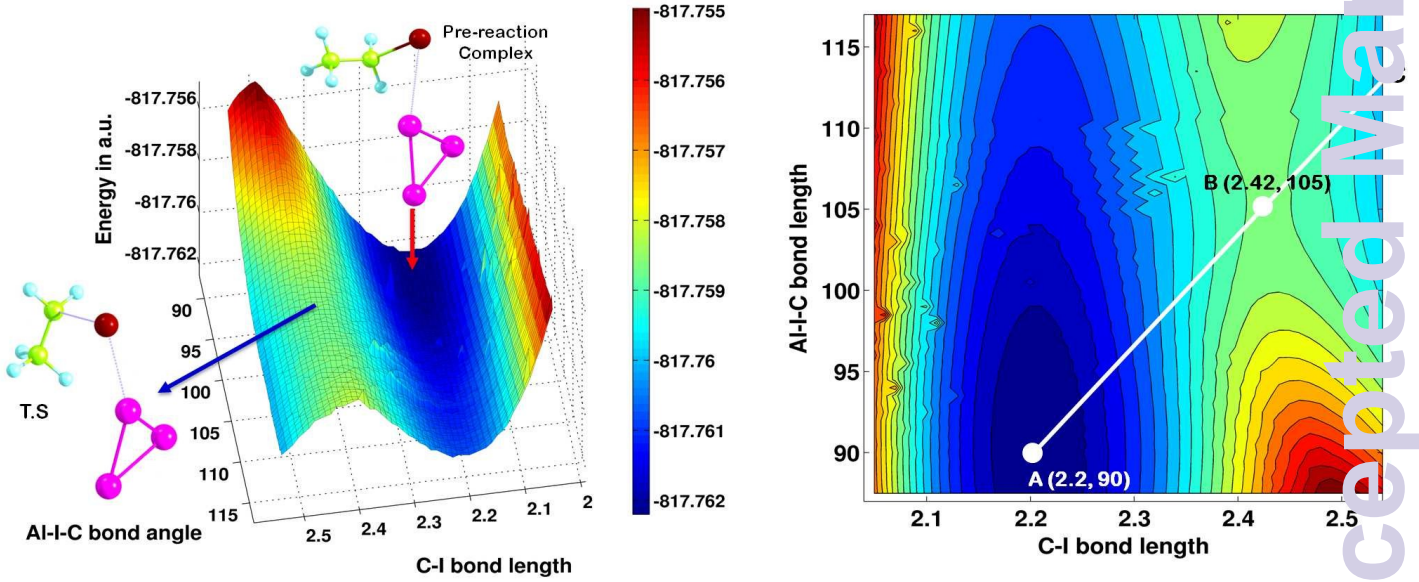

Fig. 10 A segment of three dimensional potential energy surface (calculated in B3PW91 functional) for the reaction between Al_3 cluster and ethyl iodide. Contour plot for the same is given in the right hand side. The plot clearly indicates position of pre–reaction complex, transition state and the minimum energy path (MEP) towards the post–reaction complex.

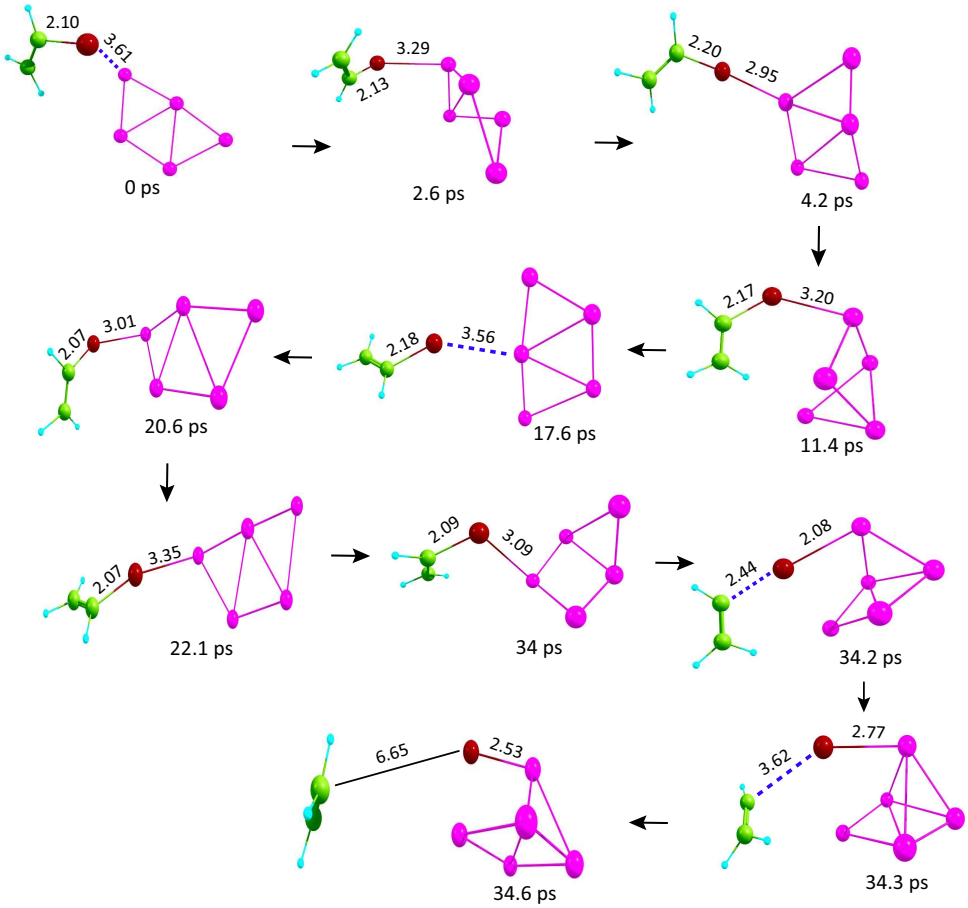

Fig. 11 Molecular dynamics (BOMD) simulation steps of C–I dissociation(iodoethene) over Al_5 cluster. Bond lengths are in *Å* and simulation time in picosecond(ps).

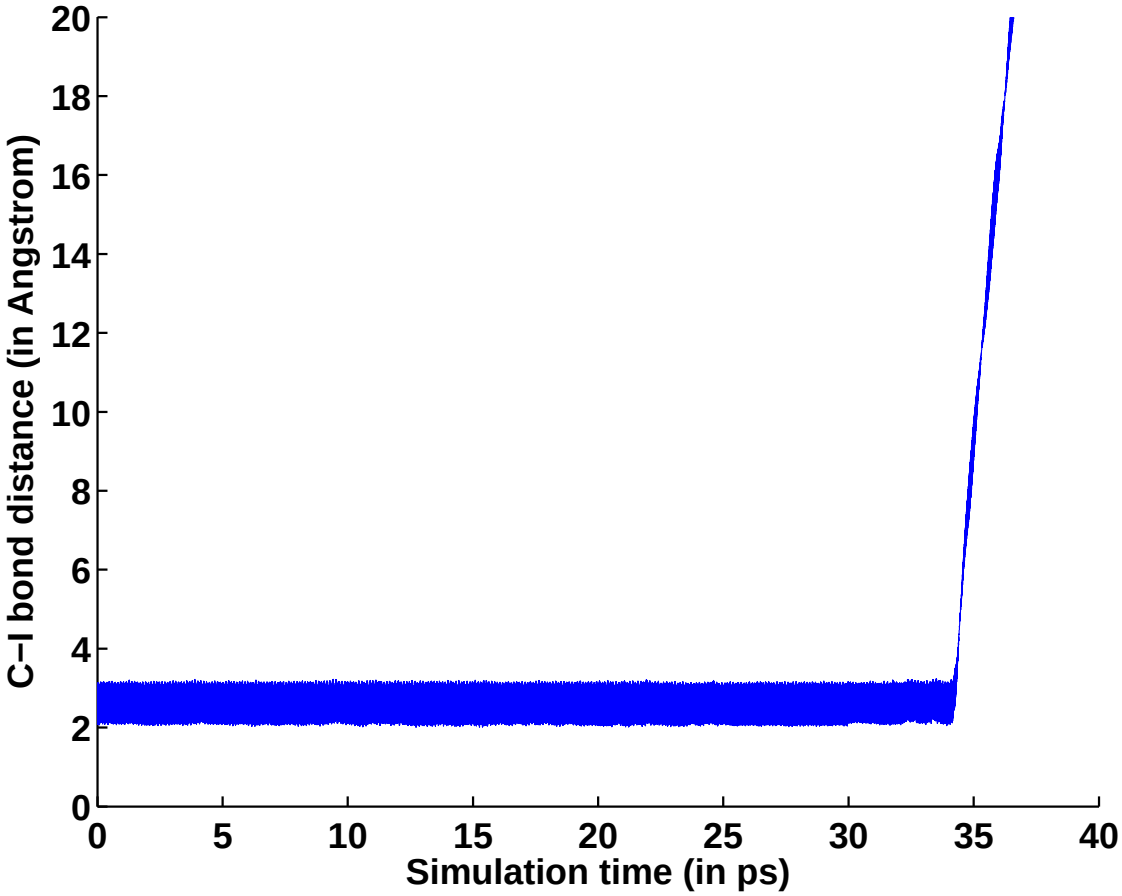

Fig. 12 C–I bond length fluctuation during BOMD simulation of Al_5–C_2H_3I complex.

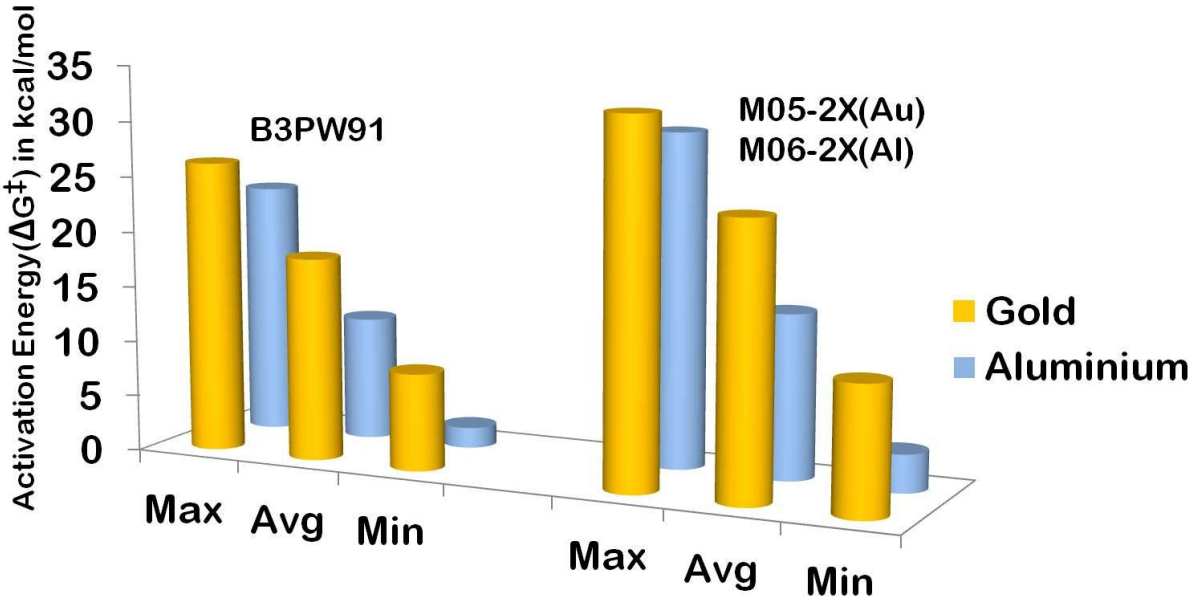

Fig. 13 Qualitative comparison of activation free energies ($\Delta G^{\ddagger}$) of aluminum with gold cluster for C–I bond dissociation in terms of activation barrier. In all aspects aluminum cluster shows better activation barrier than gold nano–clusters.

Graphical Abstract

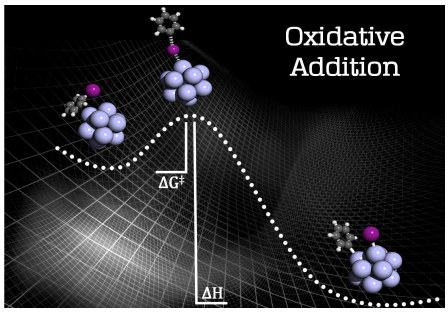

Fig. 14 Comprehensive study of the reactivities and reaction mechanism of aluminum nanoclusters towards oxidative addition of C-I bond using DFT and BOMD simulation.

Table 1 Thermodynamic data of C–I bond dissociation of ethyl iodide on Al nanoclusters in B3PW91, BHandHLYP and M06–2X functionals

Al nanoclusters	Activation Barrier (kcal mol^{-1}) $\Delta H^{\ddagger}$ B3PW91	$\Delta H^{\ddagger}$ BHandHLYP	$\Delta H^{\ddagger}$ M06–2X	$\Delta G^{\ddagger}$ B3PW91	$\Delta G^{\ddagger}$ BHandHLYP	$\Delta G^{\ddagger}$ M06–2X	Exothermicity (kcal mol^{-1}) ΔH B3PW91	ΔH BHandHLYP	ΔH M06–2X	ΔG B3PW91	ΔG BHandHLYP	ΔG M06–2X
Al_3	0.705	7.292	6.202	1.832	11.192	7.295	-68.081	-71.553	-64.846	-67.456	-68.444	-63.5[illegible]5
Al_5	5.164	11.060	9.479	7.316	14.918	10.846	-58.403	-61.849	-60.713	-56.262	-57.428	-55.827
Al_6	4.439	12.144	8.857	6.541	15.625	11.379	-47.158	-56.626	-40.552	-46.537	-54.080	-3[illegible]78
Al_7	2.841	9.640	7.709	4.036	12.238	5.483	-53.555	-57.093	-50.184	-51.612	-54.186	-[illegible].6 9
Al_8	9.413	16.282	13.711	10.632	18.397	14.737	-65.354	-69.868	-67.631	-61.816	-66.651	-66.061
Al_{13}	8.597	7.258	16.695	9.178	8.838	16.560	-45.236	-50.683	-42.455	-42.414	-46.067	[illegible]7
Al_{20}	11.469	16.544	18.805	13.644	18.306	20.031	-48.776	-55.676	-47.731	-48.232	-54.399	-46.4[illegible]0

Table 2 Rate constants and binding energies for C–I bond dissociation of ethyl iodide on Al nanoclusters in B3PW91, BHandHLYP and M06–2X functionals

Al nanoclusters	E.P Rate constant BHandHLYP	M06–2X	B3PW91	Binding Energy(kcal mol^{-1}) ΔE(M06–2X)	ΔE_{BSSE}(M06–2X)
Al_3	$2.815x10^{11}$	$3.845x10^{4}$	$2.772x10^{7}$	-5.005	-4.348
Al_5	$2.677x10^{7}$	$7.124x10^{1}$	$6.901x10^{4}$	-4.338	-3.786
Al_6	$9.909x10^{7}$	$2.155x10^{1}$	$2.804x10^{4}$	-9.805	-8.923
Al_7	$6.809x10^{9}$	$6.573x10^{3}$	$5.907x10^{8}$	-1.856	-0.838
Al_8	$9.904x10^{4}$	$1.999x10^{-1}$	$9.656x10^{1}$	-6.987	-5.938
Al_{13}	$1.154x10^{6}$	$2.047x10^{6}$	$4.445x10^{0}$	-4.781	-3.919
Al_{20}	$6.122x10^{2}$	$2.331x10^{-1}$	$1.267x10^{-2}$	-9.491	-8.393

Table 3 Thermodynamic data of C–I bond dissociation of ethylene iodide on Al nanoclusters in B3PW91, BHandHLYP and M06–2X functionals

Al nanoclusters	Activation Barrier(in kcal mol^{-1}) $\Delta H^{\ddagger}$ B3PW91	$\Delta H^{\ddagger}$ BHandHLYP	$\Delta H^{\ddagger}$ M06–2X	$\Delta G^{\ddagger}$ B3PW91	$\Delta G^{\ddagger}$ BHandHLYP	$\Delta G^{\ddagger}$ M06–2X	Exothermicity(kcal mol^{-1}) ΔH B3PW91	ΔH BHandHLYP	ΔH M06–2X	ΔG B3PW91	ΔG BHandHLYP	ΔG B3PW91
Al_3	4.006	6.826	8.791	3.863	8.654	9.586	-73.791	-77.766	-69.935	-72.377	-74.146	-68.[illegible]29
Al_5	3.41	6.946	7.87	5.87	10.094	9.37	-60.89	-65.742	-63.84	-56.65	-60.636	-61.[illegible]4
Al_6	19.389	27.248	25.621	21.205	30.240	26.141	-51.935	-61.309	-49.841	-50.561	-58.799	-[illegible]87
Al_7	0.0119	4.095	3.465	2.792	6.332	3.4142	-49.237	-51.670	-48.396	-43.689	-47.857	-4[illegible]10
Al_8	13.181	22.654	16.330	16.192	27.652	19.013	-70.875	-76.372	-74.621	-68.449	-71.590	-[illegible]3
Al_{13}	15.575	6.025	13.344	14.765	9.963	14.297	-48.890	-55.785	-45.624	-46.921	-50.573	-[illegible]18
Al_{20}	18.830	27.634	23.864	22.645	29.934	24.625	-54.431	-62.086	-53.145	-51.850	-59.805	-[illegible]03

Table 4 Rate constants and binding energies for C–I bond dissociation of ethylene iodide on Al nanoclusters in B3PW91, BHandHLYP and M06–2X functionals

Al nanoclusters	E.P Rate constant			Binding Energy(kcal mol^{-1})	
	B3PW91	BHandHLYP	M06–2X	ΔE(M06–2X)	ΔE_{BSSE}(M06–2X)
Al_3	$9.121x10^{9}$	$2.792x10^{6}$	$5.788x10^{5}$	-4.414	-3.927
Al_5	$3.077x10^{8}$	$2.456x10^{5}$	$8.343x10^{5}$	-3.351	-2.976
Al_6	$1.744x10^{-3}$	$4.131x10^{-10}$	$4.188x10^{-7}$	-8.389	-7.607
Al_7	$5.567x10^{10}$	$1.410x10^{8}$	$1.946x10^{10}$	-2.146	-1.904
Al_8	$8.280x10^{0}$	$3.265x10^{-8}$	$7.070x10^{-2}$	-4.400	-3.642
Al_{13}	$9.221x10^{1}$	$3.065x10^{5}$	$2.031x10^{2}$	-3.599	-2.976
Al_{20}	$1.534x10^{-4}$	$6.913x10^{-10}$	$5.418x10^{-6}$	-6.503	-5.579

Table 5 Thermodynamic data of C–I bond dissociation of benzyl iodide on Al nanoclusters in B3PW91, BHandHLYP and M06–2X functionals

Al nanoclusters	Activation Barrier (kcal mol^{-1})						Exothermicity (kcal mol^{-1})					
	$\Delta H^{\ddagger}$			$\Delta G^{\ddagger}$			ΔH			ΔG		
	B3PW91	BHandHLYP	M06–2X	B3PW91	BHandHLYP	M06–2X	B3PW91	BHandHLYP	M06–2X	B3PW91	BHandHLYP	M06–2X
Al_3	3.481	8.143	11.948	4.950	10.796	12.721	-74.692	-78.099	-67.672	-69.841	-72.341	-67.209
Al_5	3.492	6.963	8.603	5.200	11.071	8.205	-64.80	-65.956	-67.480	-61.30	-60.477	-65
Al_6	16.798	24.783	20.505	18.232	26.438	21.321	-49.720	-56.960	-46.863	-47.156	-53.253	-46.0 1
Al_7	5.029	4.237	6.803	8.708	6.666	9.926	-58.275	-61.880	-51.150	-53.974	-60.206	
Al_8	19.184	28.822	15.942	19.294	33.059	18.710	-70.119	-76.144	-71.593	69.550	-72.259	68.978
Al_{13}	16.404	11.172	17.034	14.805	13.099	16.182	-47.936	-54.385	-42.701	-47.047	-53.240	-4 .0 5
Al_{20}	22.309	29.801	26.408	21.067	31.146	29.952	-52.173	-61.441	-51.088	-54.767	-60.064	99

Table 6 Rate constants and binding energies for C–I bond dissociation of benzyl iodide on Al nanoclusters in B3PW91, BHandHLYP and M06–2X functionals

Al nanoclusters	E.P Rate constant			Binding Energy (kcal mol^{-1})	
	B3PW91	BHandHLYP	M06–2X	ΔE(M06–2X)	ΔE_{BSSE}(M06–2X)
Al_3	$1.454x10^{9}$	$7.504x10^{4}$	$2.910x10^{3}$	-6.312	-5.851
Al_5	$9.539x10^{8}$	$4.719x10^{4}$	$5.966x10^{6}$	-3.811	-3.406
Al_6	$2.642x10^{-1}$	$2.532x^{-7}$	$1.433x10^{-3}$	-8.980	-8.129
Al_7	$2.549x10^{6}$	$8.023x10^{7}$	$3.262x10^{5}$	-6.784	-6.109
Al_8	$4.398x10^{-2}$	$3.534x10^{-12}$	$1.178x10^{-1}$	-7.122	-6.394
Al_{13}	$8.612x10^{1}$	$1.536x10^{3}$	$8.425x10^{0}$	-6.907	-6.068
Al_{20}	$2.203x10^{-3}$	$8.943x10^{-11}$	$6.711x10^{-10}$	-8.800	-7.768

References

1 T. Kohei and N. Miyaura, *Cross-Coupling Reactions*, Springer, 2002, pp. 1–9.
2 N. Miyaura and S. L. Buchwald, *Cross-coupling reactions: a practical guide*, Springer, 2002, vol. 219.
3 M. G. Melchor, *A Theoretical Study of Pd-Catalyzed C-C Cross-Coupling Reactions*, Springer, 2013.
4 T. Colacot, *New Trends in Cross-Coupling: Theory and Applications*, Royal Society of Chemistry, 2014, vol. 21.
5 F. Diederich and P. J. Stang, *Metal-catalyzed cross-coupling reactions*, John Wiley & Sons, 2008.
6 I. P. Beletskaya and A. V. Cheprakov, *Coordination chemistry reviews*, 2004, **248**, 2337–2364.
7 E. Negishi, *Accounts of Chemical Research*, 1982, **15**, 340–348.
8 A. Fürstner, A. Leitner, M. Méndez and H. Krause, *Journal of the American Chemical Society*, 2002, **124**, 13856–13863.
9 A. Fürstner and R. Martin, *Chemistry Letters*, 2005, **34**, 624–629.
10 B. D. Sherry and A. Fürstner, *Accounts of chemical research*, 2008, **41**, 1500–1511.
11 G. Zhang, Y. Peng, L. Cui and L. Zhang, *Angewandte Chemie International Edition*, 2009, **48**, 3112–3115.
12 J. Han, Y. Liu and R. Guo, *Journal of the American Chemical Society*, 2009, **131**, 2060–2061.
13 C. González-Arellano, A. Abad, A. Corma, H. García, M. Iglesias and F. Sanchez, *Angewandte Chemie*, 2007, **119**, 1558–1560.
14 N. Miyaura and A. Suzuki, *Chemical reviews*, 1995, **95**, 2457–2483.
15 F. Bellina, A. Carpita and R. Rossi, *Synthesis*, 2004, **2004**, 2419–2440.
16 C. C. Johansson Seechurn, M. O. Kitching, T. J. Colacot and V. Snieckus, *Angewandte Chemie International Edition*, 2012, **51**, 5062–5085.
17 K. Tamao, K. Sumitani and M. Kumada, *Journal of the American Chemical Society*, 1972, **94**, 4374–4376.
18 R. F. Heck, *Palladium reagents in organic syntheses*, Academic Press London, 1985, vol. 6.
19 K. Sonogashira, *Journal of organometallic chemistry*, 2002, **653**, 46–49.
20 A. King, N. Okukado and E. Negishi, *Journal of the Chemical Society, Chemical Communications*, 1977, 683–684.
21 J. K. Stille, *Angewandte Chemie International Edition in English*, 1986, **25**, 508–524.
22 A. Suzuki, *Journal of Organometallic Chemistry*, 1999, **576**, 147–168.
23 A. Molnar, *Chemical reviews*, 2011, **111**, 2251–2320.
24 P. Albers, J. Pietsch and S. F. Parker, *Journal of Molecular Catalysis A: Chemical*, 2001, **173**, 275–286.
25 J. D. Webb, S. MacQuarrie, K. McEleney and C. M. Crudden, *Journal of Catalysis*, 2007, **252**, 97–109.
26 B. M. Rosen, K. W. Quasdorf, D. A. Wilson, N. Zhang, A.-M. Resmerita, N. K. Garg and V. Percec, *Chemical reviews*, 2010, **111**, 1346–1416.
27 J. Kielhorn, C. Melber, D. Keller and I. Mangelsdorf, *International Journal of Hygiene and Environmental Health*, 2002, **205**, 417–432.
28 J. Bodnar, G. Lugosi and G. Nagy, *Process for the preparation of non-pyrophoric palladium catalysts*, US Patent 4,239,653.
29 A. Corma, R. Juárez, M. Boronat, F. Sánchez, M. Iglesias and H. García, *Chemical Communications*, 2011, **47**, 1446–1448.
30 A. Nijamudheen and A. Datta, *The Journal of Physical Chemistry C*, 2013, **117**, 21433–21440.
31 S. Khanna and P. Jena, *Physical review letters*, 1992, **69**, 1664.
32 S. N. Khanna and P. Jena, *Physical Review B*, 1995, **51**, 13705.
33 N. Jones, J. U. Reveles, S. Khanna, D. Bergeron, P. Roach and A. Castleman Jr, *The Journal of chemical physics*, 2006, **124**, 154311.
34 D. Cox, D. Trevor, R. Whetten and A. Kaldor, *The Journal of Physical Chemistry*, 1988, **92**, 421–429.
35 M. F. Jarrold and J. E. Bower, *Journal of the American Chemical Society*, 1988, **110**, 70–78.
36 W. H. Woodward, N. Eyet, N. S. Shuman, J. C. Smith, A. A. Viggiano and A. Castleman Jr, *The Journal of Physical Chemistry C*, 2011, **11**[illegible] 9903–9908.
37 B. S. Kulkarni, S. Krishnamurty and S. Pal, *The Journal of Physical Chemistry C*, 2011, **115**, 14615–14623.
38 S. Das, S. Pal and S. Krishnamurty, *The Journal of Physical Chemistry C*, 2014, **118**, 19869–19878.
39 R. Burgert, H. Schnöckel, A. Grubisic, X. Li, S. T. Stokes, K. H. Bowen, G. Ganteför, B. Kiran and P. Jena, *Science*, 2008, **319**, 438–442.
40 M. Neumaier, M. Olzmann, B. Kiran, K. H. Bowen, B. Eichhorn, S. T. Stokes, A. Buonaugurio, R. Burgert and H. Schnockel, *Journal of the American Chemical Society*, 2014, **136**, 3607–3616.
41 R. Burgert and H. Schnöckel, *Chemical Communications*, 2008, 2075–2089.
42 D. Bergeron and A. Castleman, *Chemical physics letters*, 2003, **371**, 189–193.
43 S. Mezhenny, D. C. Sorescu, P. Maksymovych and J. T. Yates, *Journal of the American Chemical Society*, 2002, **124**, 14202–14209.
44 D. E. Bergeron, A. W. Castleman, T. Morisato and S. N. Khanna, *Science*, 2004, **304**, 84–87.
45 P. Clayborne, N. O. Jones, A. C. Reber, J. U. Reveles, M. Qian and S. N. Khanna, *Journal of Computational Methods in Science and Engineering*, 2007, **7**, 417–430.
46 A. C. Reber, S. N. Khanna and A. W. Castleman, *Journal of the American Chemical Society*, 2007, **129**, 10189–10194.
47 D. Bergeron, P. Roach, A. Castleman, N. Jones and S. Khanna, *Science*, 2005, **307**, 231–235.
48 J. U. Reveles, S. Khanna, P. Roach and A. Castleman, *Proceedings of the National Academy of Sciences*, 2006, **103**, 18405–18410.
49 W.-D. Knight, K. Clemenger, W. A. de Heer, W. A. Saunders, M. Chou and M. L. Cohen, *Physical review letters*, 1984, **52**, 2141.
50 P. Jena, *The Journal of Physical Chemistry Letters*, 2015, **6**, 1549–1552.
51 R. Burgert, S. T. Stokes, K. H. Bowen and H. Schnöckel, *Journal of the American Chemical Society*, 2006, **128**, 7904–7908.
52 R. Burgert, H. Schnöckel, M. Olzmann and K. H. Bowen, *Angewandte Chemie International Edition*, 2006, **45**, 1476–1479.
53 S. Kozuch and S. Shaik, *Journal of the American Chemical Society*, 2006, **128**, 3355–3365.
54 S. J. Blanksby and G. B. Ellison, *Accounts of Chemical Research*, 2003, **36**, 255–263.
55 M. J. Frisch, G. W. Trucks, H. B. Schlegel, G. E. Scuseria, M. A. Robb, J. R. Cheeseman, G. Scalmani, V. Barone, B. Mennucci, G. A. Petersson, H. Nakatsuji, M. Caricato, X. Li, H. P. Hratchian, A. F. Izmaylov, J. Bloino, G. Zheng, J. L. Sonnenberg, M. Hada, M. Ehara, K. Toyota, R. Fukuda, J. Hasegawa, M. Ishida, T. Nakajima, Y. Honda, O. Kitao, H. Nakai, T. Vreven, J. J. A. Montgomery, J. E. Peralta, F. Ogliaro, M. Bearpark, J. J. Heyd, E. Brothers, K. N. Kudin, V. N. Staroverov, R. Kobayashi, J. Normand, K. Raghavachari, A. Rendell, J. C. Burant, S. S. Iyengar, J. Tomasi, M. Cossi, N. Rega, J. M. Millam, M. Klene, J. E. Knox, J. B. Cross, V. Bakken, C. Adamo, J. Jaramillo, R. Gomperts, R. E. Stratmann, O. Yazyev, A. J. Austin, R. Cammi, C. Pomelli, J. W. Ochterski, R. L. Martin, K. Morokuma, V. G. Zakrzewski, G. A. Voth, P. Salvador, J. J. Dannenberg, S. Dapprich, A. D. Daniels, Ö. Farkas, J. B. Foresman, J. V. Ortiz, J. Cioslowski and D. J. Fox, *Gaussian09 Revision D.01*, Gaussian Inc. Wallingford CT 2009.
56 S. F. Boys and F. d. Bernardi, *Molecular Physics*, 1970, **19**, 553–566.
57 H. Eyring, *The Journal of Chemical Physics*, 1935, **3**, 107–115.
58 H. Eyring, *Chemical Reviews*, 1935, **17**, 65–77.
59 M. G. Evans and M. Polanyi, *Trans. Faraday Soc.*, 1935, **31**, 875–894.
60 A. Köster, P. Calaminici, M. Casida, R. Flores-Moreno, G. Geudtner, A. Goursot, T. Heine, A. Ipatov, F. Janetzko, J. del Campo *et al.*
61 H. J. Berendsen, J. P. M. Postma, W. F. van Gunsteren, A. DiNola and

J. Haak, *The Journal of chemical physics*, 1984, **81**, 3684–3690.
62 A. M. Köster, J. U. Reveles and J. M. del Campo, *The Journal of chemical physics*, 2004, **121**, 3417–3424.
63 J. A. Alonso *et al.*, *Structure and properties of atomic nanoclusters*, World Scientific, 2005.
64 E. G. Hohenstein, S. T. Chill and C. D. Sherrill, *Journal of Chemical Theory and Computation*, 2008, **4**, 1996–2000.
65 R. L. Johnston, *Atomic and molecular clusters*, CRC Press, 2002.
66 J. L. Durant, *Chemical physics letters*, 1996, **256**, 595–602.
67 A. Grubisic, X. Li, G. Gantefoer, K. H. Bowen, H. Schnöckel, F. J. Tenorio and A. Martinez, *The Journal of chemical physics*, 2009, **131**, 184305.
68 G. T. de Jong and F. M. Bickelhaupt, *Journal of Chemical Theory and Computation*, 2007, **3**, 514–529.